JACS
JOURNAL OF THE AMERICAN CHEMICAL SOCIETY
pubs.acs.org/JACS
Article

Solvation Structure Design for Aqueous Zn Metal Batteries

Longsheng Cao,[#] Dan Li,[#] Enyuan Hu, Jijian Xu, Tao Deng, Lin Ma, Yi Wang, Xiao-Qing Yang, and Chunsheng Wang*

Cite This: https://dx.doi.org/10.1021/jacs.0c09794
Read Online

ABSTRACT: Aqueous Zn batteries are promising energy storage devices for large-scale energy-storage due to low cost and high energy density. However, their lifespan is limited by the water decomposition and Zn dendrite growth. Here, we suppress water reduction and Zn dendrite growth in dilute aqueous electrolyte by adding dimethyl sulfoxide (DMSO) into $ZnCl_2$–H_2O, in which DMSO replaces the H_2O in Zn^{2+} solvation sheath due to a higher Gutmann donor number (29.8) of DMSO than that (18) of H_2O. The preferential solvation of DMSO with Zn^{2+} and strong H_2O–DMSO interaction inhibit the decomposition of solvated H_2O. In addition, the decomposition of solvated DMSO forms $Zn_{12}(SO_4)_3Cl_3(OH)_{15}$·$5H_2O$, $ZnSO_3$, and ZnS enriched-solid electrolyte interphase (SEI) preventing Zn dendrite and further suppressing water decomposition. The $ZnCl_2$–H_2O–DMSO electrolyte enables Zn anodes in Zn||Ti half-cell to achieve a high average Coulombic efficiency of 99.5% for 400 cycles (400 h), and the Zn||MnO_2 full cell with a low capacity ratio of Zn:MnO_2 at 2:1 to deliver a high energy density of 212 Wh/kg (based on both cathode and anode) and maitain 95.3% of the capacity over 500 cycles at 8 C.

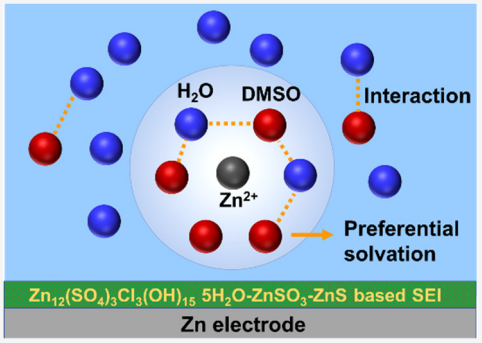

INTRODUCTION

Metallic zinc (Zn) is an ideal anode material for aqueous batteries because of its high theoretical capacity (5851 mAh mL^{-1} and 820 mA h g^{-1}), low redox potential (−0.76 V versus the standard hydrogen electrode), high abundance, water compatibility, and intrinsic safety.[1−6] However, the reaction of Zn anodes with water in aqueous electrolytes reduces Coulombic efficiency (CE), consumes water and Zn, and promotes Zn dendrite growth.[7−10]

Parasitic water reduction during Zn deposition is accelerated by the high overpotential associated with strong Coulombic interactions between the solvated Zn^{2+} ion and its surrounding H_2O shell.[9−11] The increase in local pH envirment due to H_2 evolution promotes the formation of Zn^{2+}-insulating passivate layer (such as Zn hydroxides) on the Zn surface,[12,13] reducing the Zn utilization and cycle life, and promoting Zn dendrite growth.[14,15] To suppress the water reduction and Zn dendrite, the bonding strength between Zn^{2+} ion and solvated H_2O should be weakened, and a uniform Zn-ion conductive solid electrolyte interphase (SEI) has to be constructed, which allows Zn^{2+} transport while preventing H_2O from penetration to Zn anode surface. To weaken the bonding strength between Zn^{2+} ion and H_2O, Wang et al.[7] developed a 21 m LiTFSI–H_2O–1 m $Zn(TFSI)_2$ water-in-salt, where the support Li^+ strongly bonds with H_2O, while Zn^{2+} ions are closely coordinated with $TFSI^-$ rather than H_2O, thus significantly reducing the H_2O activity in the electrolyte. Ji et al.[16] developed a 30 m $ZnCl_2$–H_2O–5 m LiCl water-in-salt, where the hydrogen bonding network of water is interrupted and Zn^{2+} ions are closely coordinated with Cl^- rather than H_2O, thus strenghening O–H covalent bonds and decreasing H_2O activity in the electrolyte. Chen et al.[17] reported a 7.5 m $ZnCl_2$ electrolyte with interrupted hydrogen bonding network of water and decreased H_2O activity at −70 °C. Adding salt concentration can effectvely weaken the bonding between Zn^{2+} and H_2O, thus suppressing the water decomposition during Zn deposition. However, the high cost and high viscosity of the water-in-salt electrolytes remain unsolved.[18,19] Alternatively, the H_2O reduction on Zn can also be prevented by forming a ZnF_2–$Zn_3(PO_4)_2$ SEI through a hydrophobic organic electrolyte surface coating.[20] However, the complex surface coating of the organic layer electrolyte limits its large-scale application. It is highly desired to form SEI and reduce the H_2O activity by simply adding additives into aqueous electrolytes. Liu and Pan et al.[21] added poly(ethylene oxide) polymer (PEO) as additive into $ZnSO_4$, where ether groups of PEO interact strongly with Zn^{2+} ions and PEO molecules adsorbed onto Zn anodes. However, Zn^{2+} ion transfer kinetics and power density are seriously reduced, although H_2 generation on Zn metal anode is suppressed. The electrolyte additive should satisfy three stringent requirments: (1) The solvent additive should have a

Received: September 13, 2020

higher Gutmann donor number than H_2O enabling it to replace the H_2O in the Zn^{2+} solvation sheath without seriously sacrificing Zn^{2+} ion transfer kinetics. (2) It should be able to form a strong bond with H_2O to reduce H_2O activity and suppress H_2O reduction. (3) It should be able to from a dense and self-repairable solid−electrolyte interphase (SEI) to prevent water penetration onto Zn anode.

Dimethyl sulfoxide (DMSO) has high dielectric constant, high donor number (29.8), and low cost,[22] which can preferentially solvate with Zn ions and exclude water from Zn^{2+} solvation sheath. Besides, DMSO also has a strong interaction to water, reducing the water activity.[23] DMSO has been added into alkaline,[24] organic,[25] and ionic liquid−H_2O[26] Zn-ion electrolyte to suppress zinc dendrite formation. In alkaline zinc−air battery,[24] the DMSO inhibited the passivation of zinc surface enhancing the zinc dissolution/deposition. In organic[25] or ionic liquid-H_2O[26] zinc batteries, the DMSO also enhanced the reversibility of Zn plating/stripping. However, the Zn dendrite suppression mechanism of DMSO in these electrolytes remains unexplored and DMSO has not been added into neutral aqueous electrolytes, which are the most promising electrolytes for aqueous Zn batteries.

Here, we added dimethyl sulfoxide (DMSO) additive into a dilute aqueous 1.6 m $ZnCl_2$−H_2O (mole ratio of $ZnCl_2$:H_2O = 1:34) electrolyte forming a 1.3 m $ZnCl_2$/H_2O−DMSO (volume ratio of H_2O/DMSO = 4.3:1) electrolyte. Since the donor number (29.8) of DMSO is much higher than that (18) of H_2O[22] and preferential conscription of cosolvents in the structure of the solvation sheath of Li ions,[10] the H_2O solvated Zn^{2+} sheath was altered by preferential solvation of DMSO (Figure 1). The preference reduction of DMSO during Zn deposition forms a dense $Zn_{12}(SO_4)_3Cl_3(OH)_{15}\cdot 5H_2O$−$ZnSO_3$−ZnS solid electrolyte interphase, inhibiting the decomposition of solvated H_2O. In addition, the water activity was further decreased due to the stronger H_2O−DMSO interactions. The combination of reducing H_2O activity and forming SEI significantly enhances the Zn plating/stripping CE to ∼100% for up to 400 cycles (400 h). Leveraging this high reversibility, Zn||MnO_2 batteries with P/N capacity ratio of 1:2 retain 95.3% of the initial capacity after 500 cycles.

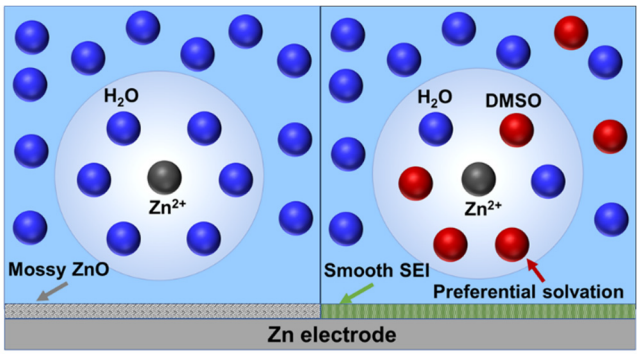

Figure 1. Scheme of Zn^{2+} solvation structure and zinc surface passivation in H_2O (left) and H_2O−DMSO (right) solvents.

RESULTS AND DISCUSSION

Solvation Structure of $ZnCl_2$−H_2O−DMSO Electrolyte. Adding 20 wt % of DMSO into $ZnCl_2$−H_2O electrolyte significantly suppressed the electrochemical water decomposition, as evidenced by a much lower hydrogen evolution current in 1.3 m $ZnCl_2$−H_2O−DMSO electrolyte than that in 1.6 m $ZnCl_2$−H_2O during the linear cathodic potential scan of an inert titanium electrode after the activation process (Figure S1). At −0.02 V vs Zn/Zn^{2+}, the reduction current reduced from −16 μA (Zn + H_2) to −13 μA (Zn plating), as confirmed by almost 100% Coulombic efficiency of Zn plating/stripping in $ZnCl_2$−H_2O−DMSO due to the formation of $Zn_{12}(SO_4)_3Cl_3(OH)_{15}\cdot 5H_2O$−$ZnSO_3$−ZnS SEI. In addition, oxidative decomposition of the electrolytes has been expanded from 2.0 to 2.2 V versus Zn/Zn^{2+} after adding DMSO into $ZnCl_2$−H_2O electrolytes.

DMSO additive reduces the bonding between Zn^{2+} and H_2O as demonstrated by X-ray absorption spectroscopy (XAS) and ft-EXAFS analysis. The edge position (when the normalized absorption coefficient is 0.5) in XAS is a good indicator of the effective charge on the atom being probed, which is Zn in this case. Edge position at higher energy indicates more effective charge. Zn XANES spectra in Figure 2a shows that the edge position obviously shifts to lower energy upon the introduction of DMSO. This indicates that the addition of DMSO leads to less electron transfer between Zn and O in H_2O or DMSO, thereby weakening the bonding strength between Zn^{2+} and H_2O in the Zn^{2+} solvation sheath. More solvation structure information is also revealed by the ft-EXAFS shown in Figure 2b, indicating that the solvation structure is mostly limited to the first shell, which corresponds to the first and the strongest peak (Zn−O bond). With the addition of DMSO, the Zn−O bond length increases, suggesting weakened interaction between Zn and the solvents. The decreased bonding strength between Zn^{2+} ions and H_2O is beneficial for the H_2O desolvation of Zn^{2+} during the Zn plating process, inhibiting H_2O reduction and hence increasing Zn plating/stripping Coulombic efficiency.

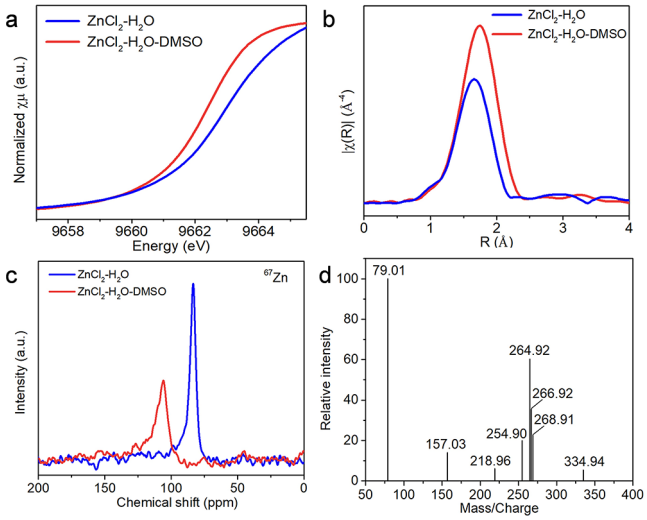

Figure 2. (a) X-ray absorption near-edge structure (XANES) and (b) Fourier transformed extended X-ray absorption fine structure (ft-EXAFS) spectra of $ZnCl_2$−H_2O−DMSO and $ZnCl_2$−H_2O electrolytes. (c) ^{67}Zn nuclear magnetic resonance (NMR) spectra in $ZnCl_2$−H_2O−DMSO and $ZnCl_2$−H_2O electrolytes. (d) Ionic high resolution mass spectra (HRMS) of $ZnCl_2$−H_2O−DMSO, showing the presence of a number of cationic Zn complexes $[Zn(H_2O)_4(OH)_3(DMSO)]^-$ (m/z = 265, 267, 269).

^{67}Zn NMR spectroscopy demonstrated that DMSO participates in Zn^{2+} solvation sheath. Even with a small

https://dx.doi.org/10.1021/jacs.0c09794
J. Am. Chem. Soc. XXXX, XXX, XXX−XXX

DMSO:H_2O molar ratio of 1:17, the ^{67}Zn chemical shift of $ZnCl_2$−H_2O−DMSO (106 ppm) is significantly larger than that of $ZnCl_2$−H_2O electrolyte (83 ppm) (Figure 2c), indicating the deshielding effect of the solvation sheath on Zn^{2+} ions. This is because that DMSO is involved in solvation sheath to replace some H_2O due to the higher donor number of DMSO (29.8) than that of H_2O (18)[27] and lower electron density of O in DMSO than that in H_2O (Figure S2). This result is consistent with the increased Zn−O bond length and decreased Zn−H_2O bonding strength mentioned previously.

The involvement of DMSO in the solvation structure of Zn^{2+} was also confirmed by the high-resolution mass spectra (HRMS) of $ZnCl_2$−H_2O−DMSO electrolyte. As displayed in Figure 2d, distinct signals of various DMSO-containing $[Zn(H_2O)_4(OH)_3(DMSO)]^-$ complexes at m/z = 265, 267, 269 are detected. The peak position and intensity differences of m/z for the same chemical structure are caused by the isotope pattern of Zn, including 48.6% abundance of Zn(64) in nature, 27.9% abundance of Zn(66), and 18.8% abundance of Zn(68). It should be noted that the test result is from a dilute solution in which H_2O to the $ZnCl_2$−H_2O−DMSO electrolyte volume ratio is 10^{10}:1. The strong persistence of DMSO in the Zn^{2+} solvation shell from such a dilute solution further confirms the preferential solvation effect of DMSO with Zn^{2+} compared to that of H_2O.

The strong interaction between DMSO and H_2O without interference of Zn^{2+} was confirmed using FTIR and Raman. Figure S3 indicates that the DMSO solvent displays unique stretching modes of the sulfoxide (S═O) group at around 1050 cm^{-1}. In the DMSO−H_2O mixture where the DMSO:H_2O molar ratio is 1:17, the spectral band (red line) shifts to lower wavenumbers (red shift), compared with that in pure DMSO (blue line). The red shift is attributed to the interaction between H of the O−H bond in water molecules and O of the S═O double bond in DMSO (S═O···H−O). Strong interaction between DMSO and H_2O was also confirmed by the difference in thermal stabilities of $ZnCl_2$−H_2O−DMSO and $ZnCl_2$−H_2O electrolytes. As shown in thermal gravimetric analysis (TGA) curves (Figure S4), the addition of DMSO into $ZnCl_2$−H_2O effectively suppresses the H_2O evaporation by increasing the evaporation ending temperature (EET) from 67 to 95 °C, due to strong interaction between DMSO and Zn^{2+}. This interaction contributes to the decreased interaction between H_2O and Zn^{2+}. In addition, the strong interaction between DMSO and Zn^{2+} slightly decreases the conductivity to 42.1 from 70.8 mS cm^{-1} of the $ZnCl_2$−H_2O electrolyte. In summary, DMSO replaces H_2O in Zn^{2+} solvation sheath, weakening the bonding between Zn^{2+} and H_2O. DMSO itself also strongly bonds to H_2O, reducing the H_2O activity. The synthetic impacts of DMSO promote the DMSO reduction but suppress H_2O reduction, forming a robust SEI.

Electrochemical Performance of Zn Anode in $ZnCl_2$−H_2O−DMSO Electrolyte. The stability of the Zn anode in $ZnCl_2$−H_2O electrolytes with and without DMSO was evaluated at a current of 0.5 mA cm^{-2} and a capacity of 0.5 mAh/cm^2 using symmetrical Zn||Zn cells (Figure 3a). In the $ZnCl_2$−H_2O electrolyte, the Zn||Zn cell only shows a stable cycle for 390 h with ∼20.0 mV overpotential. After that, the sudden and irreversible rise of the polarization voltage appeared, and then the cell failed due to Zn dendrite growth. In contrast, the Zn||Zn cell in $ZnCl_2$−H_2O−DMSO exhibits a stable polarization overpotential of ∼20.5 mV and an ultralong

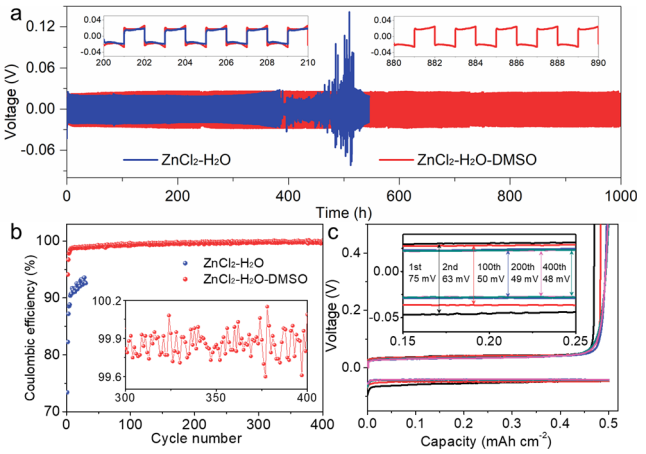

Figure 3. (a) Galvanostatic Zn plating/stripping in Zn||Zn symmetrical cells at a current density of 0.5 mA cm^{-2} and a capacity of 0.5 mAh cm^{-2}. (b) Zn plating/stripping Coulombic efficiency in different electrolytes at 1 mA cm^{-2} and 0.5 mAh cm^{-2}. (c) Voltage profiles of Zn plating/stripping processes at selected cycles in $ZnCl_2$−H_2O−DMSO electrolytes.

cycling life of 1000 h, which is a 2.5-fold improvement in cycle life. Although introducing DMSO slightly reduced the ionic conductivity and increased the SEI resistance, the overall resistance of the Zn anode in $ZnCl_2$−H_2O−DMSO electrolytes is similar to that in the $ZnCl_2$−H_2O electrolyte due to fast charge-transfer reaction (Figure S5). At the same capacity, when the current increases from 0.5 to 10 mA/cm^2, both cells show an increased overpotential for Zn plating/stripping (Figure S6). However, the overpotential of Zn plating/stripping gradually reduces with cycles.

To achieve a high energy density, the Zn mass should be minimized, which requires a high Coulombic efficiency (CE). Zn||Ti coin-type cells were employed to evaluate the CE of Zn plating/stripping (Figure 3b, Figure S7). Zn||Ti half-cell in the $ZnCl_2$−H_2O electrolyte shows a fluctuant voltage signals with a low average CE of ∼90.7% (Figure 3b, Figure S8). In contrast, the Zn||Ti half-cell in the $ZnCl_2$−H_2O−DMSO electrolyte shows a high average CE of 99.5%. Specifically, the zinc plating/stripping CE improves to 99.0% within 30 cycles due to the formation of robust SEI and ultimately reached a high CE of ∼100% with a steady overpotential of ∼24 mV (Figure 3b,c), which is one of the best performances among all reported Zn anodes.[7,16,17,21] The universality of DMSO additives for enhancing the CE of Zn plating/stripping was further confirmed using 1.0 m $Zn(OTF)_2$ aqueous electrolyte. The Zn||Ti cell without DMSO additive showed a low CE (∼93%) and short-circuit occurred after only 25 cycles. In contrast, adding 20 wt % of DMSO additive into 1.0 m $Zn(OTF)_2$ aqueous electrolyte increased the CE to 99.3% for more than 250 cycles (Figure S9).

The zinc electrode surface morphologies after 50 plating/stripping cycles are characterized using SEM (Figure 4). After 50 cycles, the Zn surface in $ZnCl_2$−H_2O electrolyte becomes rough with flake-like dendrites (Figure 4a−c) due to continuous reactions between Zn and aqueous electrolyte, as evidenced by a low CE (∼90.7%) and poor cycling stability. In contrast, the Zn cycled in $ZnCl_2$−H_2O−DMSO electrolyte shows a dense and smooth morphology (Figure 4d−f), confirmed by the uniform S and Cl elements distribution (Figure S10). The thickness of the cycled Zn in $ZnCl_2$−H_2O

https://dx.doi.org/10.1021/jacs.0c09794
J. Am. Chem. Soc. XXXX, XXX, XXX−XXX

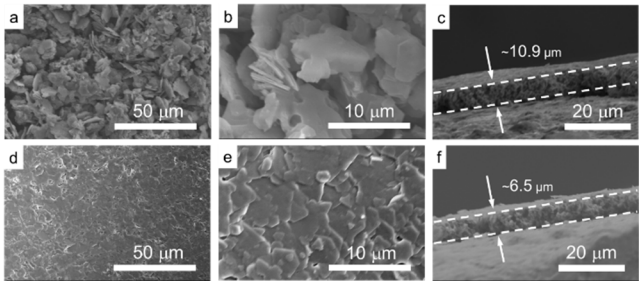

Figure 4. SEM images of Zn electrodes in Zn||Zn symmetrical cells after 50 plating/stripping cycles at 0.5 mA cm^{-2} and 0.5 mAh cm^{-2} in (a–c) $ZnCl_2$–H_2O and (d–f) $ZnCl_2$–H_2O–DMSO electrolytes. In c and f, white lines indicated the etching depth in cross-section view.

electrolyte is 10.9 μm, and was reduced to 6.5 μm when it was cycled in $ZnCl_2$–H_2O–DMSO (white lines in Figure 4c and f). Therefore, DMSO addition effectively suppressed water reaction with Zn anode, which suppressed Zn dendrite growth. Here, the preference reduction of solvated DMSO and suppression of H_2O reduction promote formation of a dense SEI layer on Zn surface (Figure 4f) as demonstrated by XPS and XRD below, which can further prevent water from reacting with Zn.

SEI on Zn Anode. The SEI composition on the Zn anode was analyzed using X-ray diffraction (XRD) and X-ray photoelectron spectroscopy (XPS) with an Ar^+ sputtering depth profiling characterization. XRD (Figure 5a) and optical image analysis (Figure S11) of cycled Zn anodes in $ZnCl_2$–H_2O electrolyte demonstrated that random platelet-shape Zn^{2+}-insulating $Zn_5(OH)_8Cl_2{\cdot}H_2O$ byproducts were formed on the cycled Zn electrode surface. However, Zn^{2+} conductive SEI layer was formed on Zn that cycled in $ZnCl_2$–H_2O–DMSO electrolyte as evidenced by well-identified characteristic peak of the $Zn_{12}(SO_4)_3Cl_3(OH)_{15}{\cdot}5H_2O$ and $Zn_5(OH)_6(CO_3)_2$ crystals in XRD and smooth surface in optical image (Figure S11). The detail composition distribution in SEI was also further analyzed using X-ray photoelectron spectroscopy (XPS) with an Ar^+ sputtering depth profiling (Figure 5b, Figures S12, S13, S14). S 2p spectrum in Figure 5b demonstrated that the top surface (before sputtering) of SEI formed in $ZnCl_2$–H_2O–DMSO electrolyte mainly contains inorganic $ZnSO_3$ (46%), $ZnSO_4$ (30%), and ZnS (8%) with minor organic S–C species (16%), referring to the XPS binding energy database of National Institute of Standard and Technology (NIST). During Ar^+ sputtering, the organic S–C species reduce while inorganic ZnS increase after 600 s of sputtering due to reduction of DMSO molecular decomposition during Zn deposition. Upon further sputtering to 1200 s on the Zn anode surface, the $ZnSO_4$ peak disappeared; meanwhile, the $ZnSO_3$ content plunged to ~5%, and inorganic ZnS dominated with the signal reaching ~75% of all the S signals. After 1800 s of sputtering, the inorganic ZnS content further increased to 88%. The inorganic $ZnCO_3$ signal detected from the C 1s and O 1s spectra (Figure S13), consistent with XRD spectra (Figure 5a), further confirmed the decomposition of DMSO molecules. In addition, the Cl 2p spectrum arises from two major components: inorganic chlorine from $ZnCl_2$ salt and organic chlorine from C–Cl species.[28,29] The organic chlorine could arise from reaction products between $ZnCl_2$ and DMSO, while inorganic chlorine from $ZnCl_2$ originate from the precipitation of electrolyte. The inorganic $ZnCl_2$ content increased from 77.2% at 1200 s to 93.1% at 1800 s. XPS

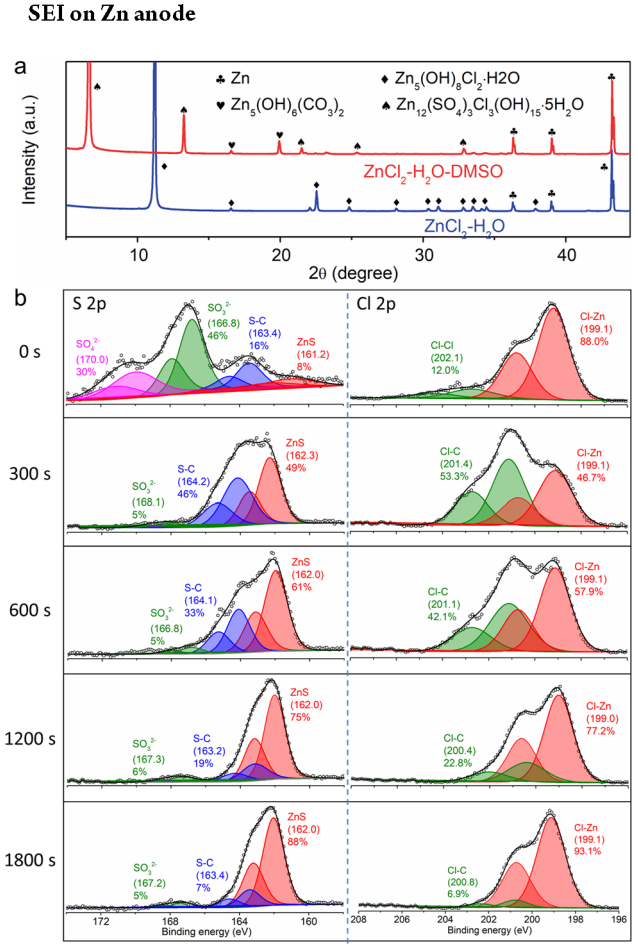

Figure 5. (a) XRD patterns of Zn anodes after plating/stripping cycles in $ZnCl_2$–H_2O–DMSO and $ZnCl_2$–H_2O electrolytes. (b) XPS characterization of the SEI formed on Zn cycled in $ZnCl_2$–H_2O–DMSO electrolyte. The S 2p and Cl 2p spectra are displayed in columns, which show the corresponding depth profiling results.

analysis demonstrated that $Zn_{12}(SO_4)_3Cl_3(OH)_{15}{\cdot}5H_2O$–$ZnSO_3$–ZnS SEI was formed on the Zn surface in $ZnCl_2$–H_2O–DMSO electrolyte, which allows Zn^{2+} to diffuse through but block the water. The contribution from DMSO to form the $Zn_{12}(SO_4)_3Cl_3(OH)_{15}{\cdot}5H_2O$–$ZnSO_3$–ZnS SEI are strongly associated with the solvation structure of Zn^{2+} ion in electrolytes.

Electrochemical Performance of MnO_2 Cathodes and Zn||MnO_2 Full Cells. The $ZnCl_2$–H_2O–DMSO electrolyte was evaluated in a Zn||MnO_2 full cell using β-MnO_2 with a tunnel structure, one of the most promising cathodes with a high theoretical capacity of 308 mAh/g for aqueous Zn batteries, and compared with that using $ZnCl_2$–H_2O aqueous electrolyte. We first evaluated the electrochemical performance of the MnO_2 cathode in two electrolytes using Zn||MnO_2 cells with excess Zn anode to reflect MnO_2 behavior. Figure 6a shows the CV response of the Zn||MnO_2 half-cell at a scan rate of 0.1 mV/s. MnO_2 in both electrolytes showed similar behavior with distinct Mn-ion redox peaks, consistent with the previous work.[30] Besides, the reduction peak at 1.15 V in the $ZnCl_2$–H_2O–DMSO electrolyte is lower than 1.22 V in $ZnCl_2$–H_2O due to the strong interaction between DMSO and Zn^{2+} and therefore sluggish interfacial Zn^{2+} charge transfer kinetics. At 0.3 C, the high CE of Zn stripping/plating and

https://dx.doi.org/10.1021/jacs.0c09794
J. Am. Chem. Soc. XXXX, XXX, XXX–XXX

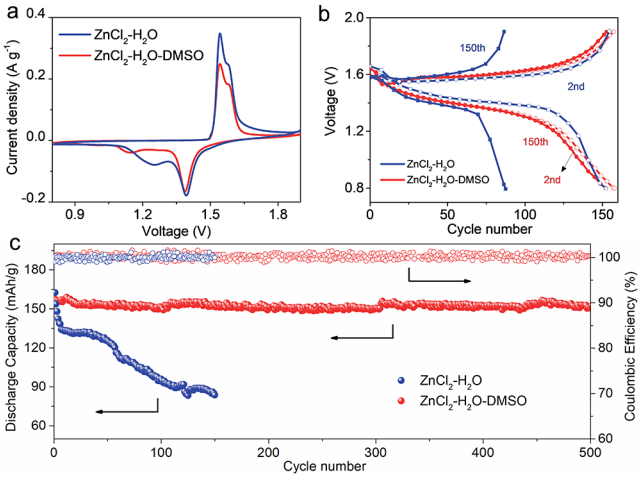

Figure 6. Electrochemical performance of Zn||MnO_2 cells. (a) CV of Zn||MnO_2 full cells at a scan rate of 0.1 mV/s. (b) Charge−discharge profiles of Zn||MnO_2 cells in $ZnCl_2$−H_2O−DMSO electrolyte. (c) Cyclic stability and efficiency of Zn||MnO_2 cells in two electrolytes with 0.1 M $MnCl_2$ to suppress Mn^{2+} dissolution at 8 C.

limited Zn anode enable a high energy density of 212 Wh kg^{-1} (based on the weight of the cathode and anode; Figure S15). The long-term cycling stability of the Zn||MnO_2 cell was evaluated at 8 C in both electrolytes with the capacity ratio of Zn:MnO_2 at 2:1 (Figure 6b,c). The Zn||MnO_2 cells in two electrolytes show a charge/discharge behavior (Figure 6b). However, the capacity of Zn||MnO_2 cells in $ZnCl_2$−H_2O electrolyte decays rapidly in 150 cycles, while the capacity of Zn||MnO_2 cells in $ZnCl_2$−H_2O−DMSO electrolyte remain stable for 500 cycles (Figure 6c). The capacity decay of Zn||MnO_2 cells in $ZnCl_2$−H_2O electrolyte is mainly attributed to the capacity decay of Zn anodes (Figure S16) and drying out of electrolytes. The Zn||MnO_2 full cell after 500 cycles in $ZnCl_2$−H_2O−DMSO electrolyte still maintained ∼150.3 mAh g^{-1}, which was 95.3% of the initial capacity with CE approaching 100%, which is one of the best performances reported to date for Zn/MnO_2 with similar P/N ratio. In contrast, the capacity of the Zn||MnO_2 cell in the $ZnCl_2$−H_2O reference electrolyte quickly dropped to 51.5% of initial capacity due to low CE for Zn plating/stripping.

CONCLUSIONS

The strong H_2O−DMSO interaction decreases the activity of solvated water and suppresses the decomposition of solvated H_2O. In addition, DMSO replaces solvated H_2O in the solvation structure of Zn^{2+} due to a high Gutmann donor number of DMSO, resulting in preferential reduction of solvated DMSO to in situ form a dense and self-repaired $Zn_{12}(SO_4)_3Cl_3(OH)_{15}$·$5H_2O$-$ZnSO_3$−ZnS SEI on Zn anodes. The SEI allows Zn^{2+} transport but blocks H_2O penetration, which further inhibits the water reduction and suppresses Zn dendrite growth. Addition of multifunctional DMSO into $ZnCl_2$−H_2O electrolytes enhances Zn plating/stripping CE to ∼100% enabling Zn||MnO_2 cells with a low capacity ratio of 2:1 to achieve a capacity retention of 95.3% of the initial capacity after 500 cycles.

ASSOCIATED CONTENT

Supporting Information

The Supporting Information is available free of charge at https://pubs.acs.org/doi/10.1021/jacs.0c09794.

Chemicals, detailed experimental methods, characterizations, and additional figures (PDF)

AUTHOR INFORMATION

Corresponding Author

Chunsheng Wang − *Department of Chemical and Biomolecular Engineering, University of Maryland, College Park, Maryland 20742, United States;* orcid.org/0000-0002-8626-6381; Email: cswang@umd.edu

Authors

Longsheng Cao − *Department of Chemical and Biomolecular Engineering, University of Maryland, College Park, Maryland 20742, United States*

Dan Li − *Department of Chemical and Biomolecular Engineering, University of Maryland, College Park, Maryland 20742, United States*

Enyuan Hu − *Chemistry Division, Brookhaven National Laboratory, Upton, New York 11973, United States;* orcid.org/0000-0002-1881-4534

Jijian Xu − *Department of Chemical and Biomolecular Engineering, University of Maryland, College Park, Maryland 20742, United States;* orcid.org/0000-0001-7727-0488

Tao Deng − *Department of Chemical and Biomolecular Engineering, University of Maryland, College Park, Maryland 20742, United States*

Lin Ma − *Department of Chemical and Biomolecular Engineering, University of Maryland, College Park, Maryland 20742, United States;* orcid.org/0000-0003-1183-1347

Yi Wang − *Department of Chemical and Biomolecular Engineering, University of Maryland, College Park, Maryland 20742, United States*

Xiao-Qing Yang − *Chemistry Division, Brookhaven National Laboratory, Upton, New York 11973, United States;* orcid.org/0000-0002-3625-3478

Complete contact information is available at: https://pubs.acs.org/10.1021/jacs.0c09794

Author Contributions

#L. Cao and D. Li contributed equally.

Notes

The authors declare no competing financial interest.

ACKNOWLEDGMENTS

C. Wang at the University of Maryland gratefully acknowledges funding support from the Advanced Research Projects Agency−Energy under Contract No. DEAR0000962. E. Hu and X.-Q. Yang at Brookhaven National Laboratory (BNL) were supported by the Assistant Secretary for Energy Efficiency and Renewable Energy, Vehicle Technology Office of the U.S. Department of Energy through the Advanced Battery Materials Research (BMR) Program under contract DE-SC0012704. This research used beamlines 7-BM of the National Synchrotron Light Source II, a U.S. DOE Office of Science User Facility operated for the DOE Office of Science by Brookhaven National Laboratory under Contract No. DE-SC0012704.

https://dx.doi.org/10.1021/jacs.0c09794
J. Am. Chem. Soc. XXXX, XXX, XXX−XXX

REFERENCES

(1) Ma, L.; Chen, S.; Li, N.; Liu, Z.; Tang, Z.; Zapien, J. A.; Chen, S.; Fan, J.; Zhi, C. Hydrogen-Free and Dendrite-Free All-Solid-State Zn-Ion Batteries. *Adv. Mater.* **2020**, *32* (14), 1908121.

(2) Wang, H.-F.; Tang, C.; Zhang, Q. A Review of Precious-Metal-Free Bifunctional Oxygen Electrocatalysts: Rational Design and Applications in Zn−Air Batteries. *Adv. Funct. Mater.* **2018**, *28* (46), 1803329.

(3) Li, B.-Q.; Zhao, C.-X.; Chen, S.; Liu, J.-N.; Chen, X.; Song, L.; Zhang, Q. Framework-Porphyrin-Derived Single-Atom Bifunctional Oxygen Electrocatalysts and their Applications in Zn−Air Batteries. *Adv. Mater.* **2019**, *31* (19), 1900592.

(4) Ji, X. A paradigm of storage batteries. *Energy Environ. Sci.* **2019**, *12* (11), 3203−3224.

(5) Mo, F.; Liang, G.; Meng, Q.; Liu, Z.; Li, H.; Fan, J.; Zhi, C. A flexible rechargeable aqueous zinc manganese-dioxide battery working at− 20° C. *Energy Environ. Sci.* **2019**, *12* (2), 706−715.

(6) Huang, J.; Wang, Z.; Hou, M.; Dong, X.; Liu, Y.; Wang, Y.; Xia, Y. Polyaniline-intercalated manganese dioxide nanolayers as a high-performance cathode material for an aqueous zinc-ion battery. *Nat. Commun.* **2018**, *9* (1), 2906.

(7) Wang, F.; Borodin, O.; Gao, T.; Fan, X.; Sun, W.; Han, F.; Faraone, A.; Dura, J. A.; Xu, K.; Wang, C. Highly reversible zinc metal anode for aqueous batteries. *Nat. Mater.* **2018**, *17* (6), 543−549.

(8) Mo, F.; Liang, G.; Meng, Q.; Liu, Z.; Li, H.; Fan, J.; Zhi, C. A flexible rechargeable aqueous zinc manganese-dioxide battery working at − 20 °C. *Energy Environ. Sci.* **2019**, *12* (2), 706−715.

(9) Blanc, L. E.; Kundu, D.; Nazar, L. F. Scientific Challenges for the Implementation of Zn-Ion Batteries. *Joule* **2020**, *4* (4), 771−799.

(10) Jin, Y.; Zou, L.; Liu, L.; Engelhard, M. H.; Patel, R. L.; Nie, Z.; Han, K. S.; Shao, Y.; Wang, C.; Zhu, J.; Pan, H.; Liu, J. Joint Charge Storage for High-Rate Aqueous Zinc−Manganese Dioxide Batteries. *Adv. Mater.* **2019**, *31* (29), 1900567.

(11) Wu, X.; Xu, Y.; Zhang, C.; Leonard, D. P.; Markir, A.; Lu, J.; Ji, X. Reverse Dual-Ion Battery via a $ZnCl_2$ Water-in-Salt Electrolyte. *J. Am. Chem. Soc.* **2019**, *141* (15), 6338−6344.

(12) Yang, H.; Chang, Z.; Qiao, Y.; Deng, H.; Mu, X.; He, P.; Zhou, H. Constructing a Super-Saturated Electrolyte Front Surface for Stable Rechargeable Aqueous Zinc Batteries. *Angew. Chem., Int. Ed.* **2020**, *59*, 9377−9381.

(13) Yang, Q.; Guo, Y.; Yan, B.; Wang, C.; Liu, Z.; Huang, Z.; Wang, Y.; Li, Y.; Li, H.; Song, L.; Fan, J.; Zhi, C. Hydrogen-Substituted Graphdiyne Ion Tunnels Directing Concentration Redistribution for Commercial-Grade Dendrite-Free Zinc Anodes. *Adv. Mater.* **2020**, *32*, 2001755.

(14) Li, Y.; Fu, J.; Zhong, C.; Wu, T.; Chen, Z.; Hu, W.; Amine, K.; Lu, J. Recent Advances in Flexible Zinc-Based Rechargeable Batteries. *Adv. Energy Mater.* **2019**, *9* (1), 1802605.

(15) Naveed, A.; Yang, H.; Shao, Y.; Yang, J.; Yanna, N.; Liu, J.; Shi, S.; Zhang, L.; Ye, A.; He, B.; Wang, J. A Highly Reversible Zn Anode with Intrinsically Safe Organic Electrolyte for Long-Cycle-Life Batteries. *Adv. Mater.* **2019**, *31* (36), 1900668.

(16) Zhang, C.; Shin, W.; Zhu, L.; Chen, C.; Neuefeind, J. C.; Xu, Y.; Allec, S. I.; Liu, C.; Wei, Z.; Daniyar, A.; Jiang, J.-X.; Fang, C.; Alex Greaney, P.; Ji, X. The electrolyte comprising more robust water and superhalides transforms Zn-metal anode reversibly and dendrite-free. *Carbon Energy* **2020**, 1−10.

(17) Zhang, Q.; Ma, Y.; Lu, Y.; Li, L.; Wan, F.; Zhang, K.; Chen, J. Modulating electrolyte structure for ultralow temperature aqueous zinc batteries. *Nat. Commun.* **2020**, *11* (1), 4463.

(18) Zhao, Z.; Zhao, J.; Hu, Z.; Li, J.; Li, J.; Zhang, Y.; Wang, C.; Cui, G. Long-life and deeply rechargeable aqueous Zn anodes enabled by a multifunctional brightener-inspired interphase. *Energy Environ. Sci.* **2019**, *12* (6), 1938−1949.

(19) Yi, J.; Liang, P.; Liu, X.; Wu, K.; Liu, Y.; Wang, Y.; Xia, Y.; Zhang, J. Challenges, mitigation strategies and perspectives in development of zinc-electrode materials and fabrication for rechargeable zinc−air batteries. *Energy Environ. Sci.* **2018**, *11* (11), 3075−3095.

(20) Cao, L.; Li, D.; Deng, T.; Li, Q.; Wang, C. Hydrophobic Organic-Electrolyte-Protected Zinc Anodes for Aqueous Zinc Batteries. *Angew. Chem., Int. Ed.* **2020**, *59*, 19292.

(21) Jin, Y.; Han, K. S.; Shao, Y.; Sushko, M. L.; Xiao, J.; Pan, H.; Liu, J. Stabilizing Zinc Anode Reactions by Polyethylene Oxide Polymer in Mild Aqueous Electrolytes. *Adv. Funct. Mater.* **2020**, *30*, 2003932.

(22) Senanayake, G.; Muir, D. M. Competitive solvation and complexation of Cu(I), Cu(II), Pb(II), Zn(II), and Ag(I) in aqueous ethanol, acetonitrile, and dimethylsulfoxide solutions containing chloride ion with applications to hydrometallurgy. *Metall. Trans. B* **1990**, *21* (3), 439−448.

(23) Nian, Q.; Wang, J.; Liu, S.; Sun, T.; Zheng, S.; Zhang, Y.; Tao, Z.; Chen, J. Aqueous Batteries Operated at − 50 °C. *Angew. Chem., Int. Ed.* **2019**, *58* (47), 16994−16999.

(24) Hosseini, S.; Abbasi, A.; Uginet, L.-O.; Haustraete, N.; Praserthdam, S.; Yonezawa, T.; Kheawhom, S. The Influence of Dimethyl Sulfoxide as Electrolyte Additive on Anodic Dissolution of Alkaline Zinc-Air Flow Battery. *Sci. Rep.* **2019**, *9* (1), 14958.

(25) Corpuz, R. D.; Juan-Corpuz, D.; Marie, L.; Nguyen, M. T.; Yonezawa, T.; Wu, H.-L.; Somwangthanaroj, A.; Kheawhom, S. Binder-Free α-MnO_2 Nanowires on Carbon Cloth as Cathode Material for Zinc-Ion Batteries. *Int. J. Mol. Sci.* **2020**, *21* (9), 3113.

(26) Xu, M.; Ivey, D. G.; Qu, W.; Xie, Z. Improved Zn/Zn(II) redox kinetics, reversibility and cyclability in 1-ethyl-3-methylimmidazolium dicyanamide with water and dimethyl sulfoxide added. *J. Power Sources* **2014**, *252*, 327−332.

(27) Kamieńska-Piotrowicz, E. Solvation of cobalt(II) and perchlorate ions in binary mixtures of donor solvents. *J. Chem. Soc., Faraday Trans.* **1995**, *91* (1), 71−75.

(28) Fiedler, R.; Herzschuh, R. An XPS investigation of the effects of heat treatment on the chlorine surface chemistry of some lignites. *Fuel* **1993**, *72* (11), 1501−1505.

(29) Wang, D.-W.; Wu, K.-H.; Gentle, I. R.; Lu, G. Q. Anodic chlorine/nitrogen co-doping of reduced graphene oxide films at room temperature. *Carbon* **2012**, *50* (9), 3333−3341.

(30) Sun, W.; Wang, F.; Hou, S.; Yang, C.; Fan, X.; Ma, Z.; Gao, T.; Han, F.; Hu, R.; Zhu, M.; Wang, C. Zn/MnO_2 Battery Chemistry With H^+ and Zn^{2+} Coinsertion. *J. Am. Chem. Soc.* **2017**, *139* (29), 9775−9778.

https://dx.doi.org/10.1021/jacs.0c09794
J. Am. Chem. Soc. XXXX, XXX, XXX−XXX